Supplementary Materials

1. Experimental Details

1.1 Methicillin-Resistant Staphylococcus aureus (MRSA) Growth Inhibition

MRSA was cultured to an optical density (OD_{600}) of 0.5 and then diluted 1000-fold in phosphate-buffered saline (PBS; 10 mM, pH 7.4). Solutions of AuCu PHNSs and AuAgCu PHNSs were prepared at concentrations of 1/20, 1/18, 1/16, 1/14, 1/12, 1/10, and 1/8 of the original stock. The experimental design consisted of two groups: a control group treated with PBS buffer and a treatment group incubated with the serially diluted nanostructures. For each condition, 100 µL of the PHNSs solution was combined with 100 µL of the diluted bacterial suspension and exposed to near-infrared (NIR) irradiation (1064 nm, 1 W cm^{-2}) for 10 min. A parallel set of samples at identical concentrations was kept in the dark for 10 min. Following treatment, 20 µL aliquots from each MRSA suspension were spread uniformly onto Luria-Bertani (LB) agar plates (n = 3 replicates per condition) and incubated at 37 °C for 16 h. Colony-forming units (CFUs) were then enumerated, and the bacterial inhibition rate was calculated using the following formula:

$$\text{Antibacterial efficiency}(\%) = \frac{C_0 - C}{C_0} \times 100\%$$

where C_0 and C represent the average CFU counts from the control (PBS-treated) and experimental groups, respectively.

1.2 Broad-Spectrum Antimicrobial Testing

A broad-spectrum evaluation was performed using the same methodology, with MRSA replaced by *Staphylococcus epidermidis*, *Streptococcus pneumoniae*, *Salmonella typhimurium*, *Escherichia coli*, and *Enterobacter cloacae*. Given its superior efficacy against MRSA, AuCu PHNSs were selected for testing against this panel at their minimum bactericidal concentration (MBC; particle concentration: 1/12 of the original stock). All other experimental conditions remained consistent with the initial MRSA assay.

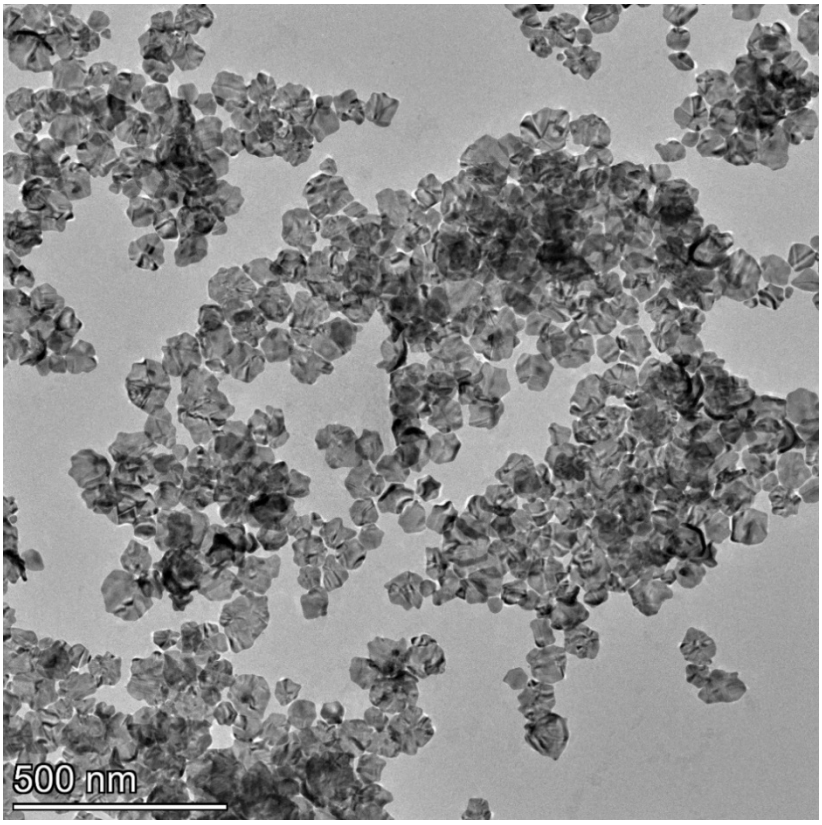

Figure S1. TEM image of Au nanoplates (NPs).

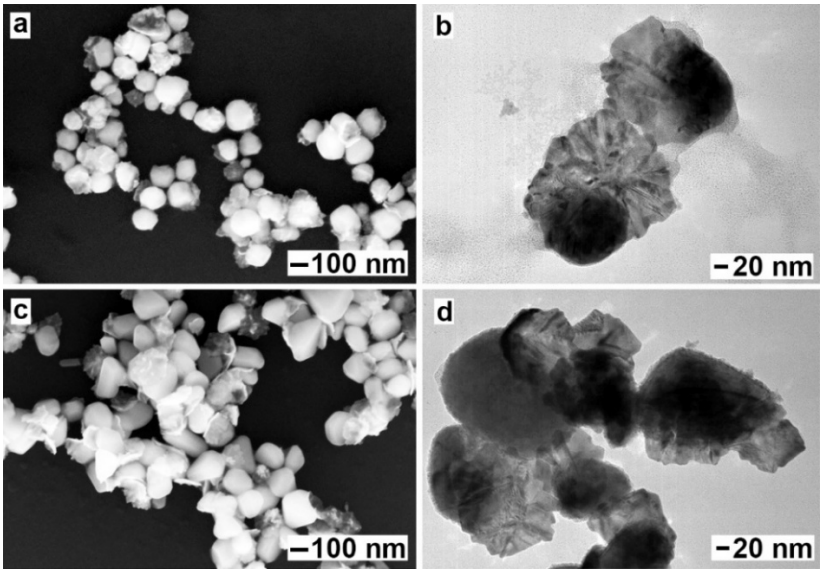

Figure S2. (**a**,**c**) SEM and (**b**,**d**) TEM images of (**a**,**b**) AuCu JNSs and (**c**,**d**) AuAgCu JNSs.

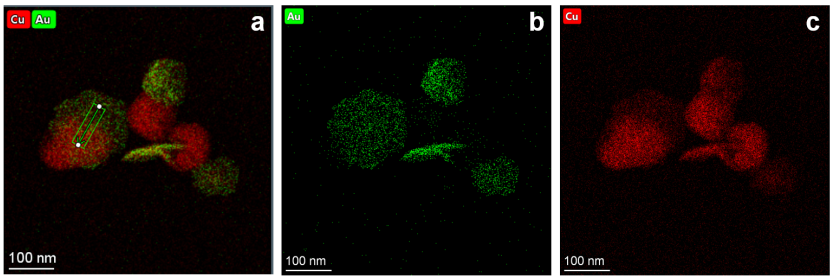

Figure S3. EDX-STEM elemental maps of the AuCu JNS: (**a**) Overlay of Au (green) and Cu (red); (**b**) Cu map; (**c**) Au map.

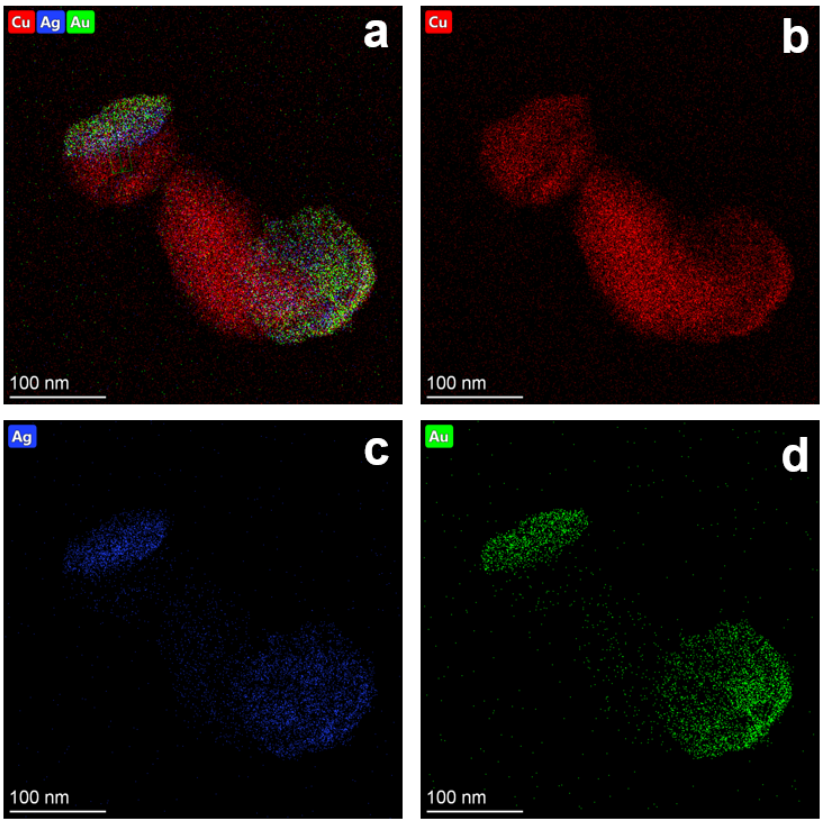

Figure S4. EDX-STEM elemental maps of the AuAgCu JNS: (**a**) Overlay of Au (green), Ag (blue), and Cu (red); (**b**) Cu map; (**c**) Ag map; (**d**) Au map.

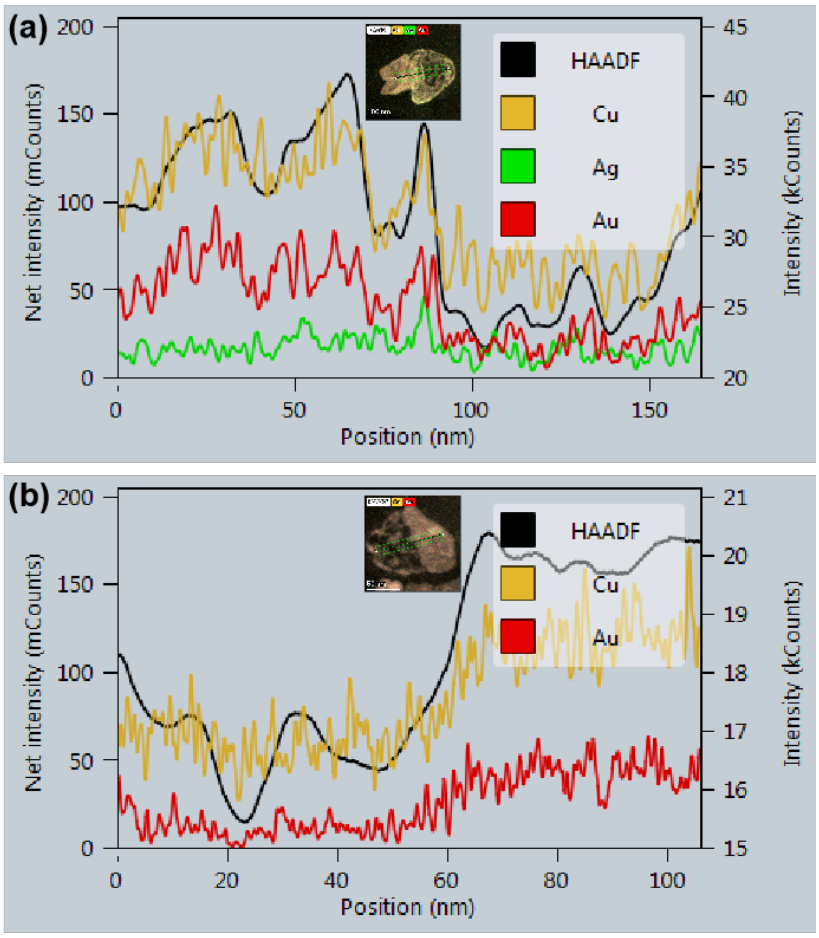

Figure S5. EDX-STEM line-scan profile: (**a**) AuAgCu PHNSs and (**b**) AuCu PHNSs.

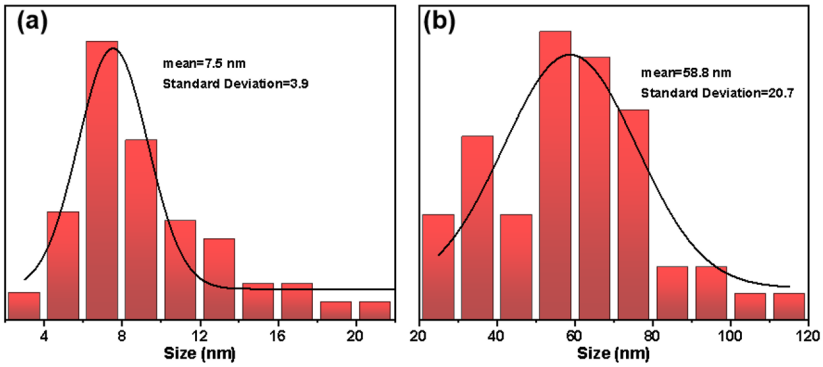

Figure S6. Histograms showing the pore size distribution of (**a**) AuAgCu PHNSs; (**b**) AuCu PHNSs.

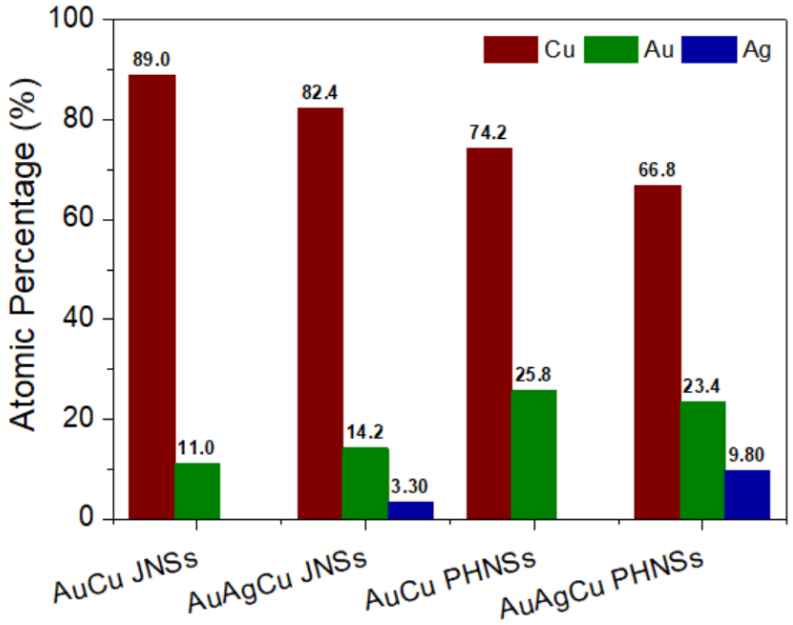

Figure S7. Histogram illustrating the atomic percentage of AuCu-based nanostructures as determined via EDS.

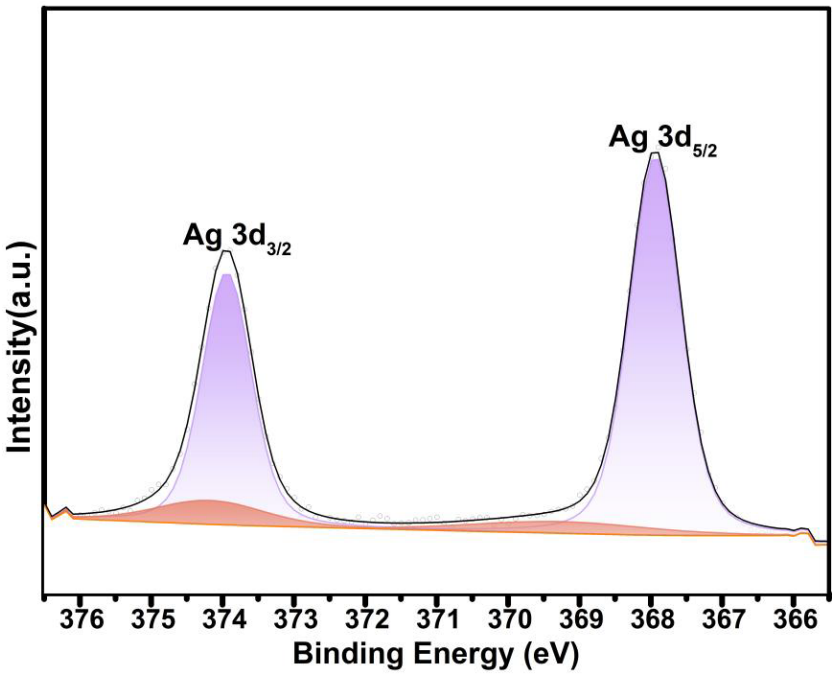

Figure S8. Ag 3d XPS spectrum of AuAgCu PHNSs.

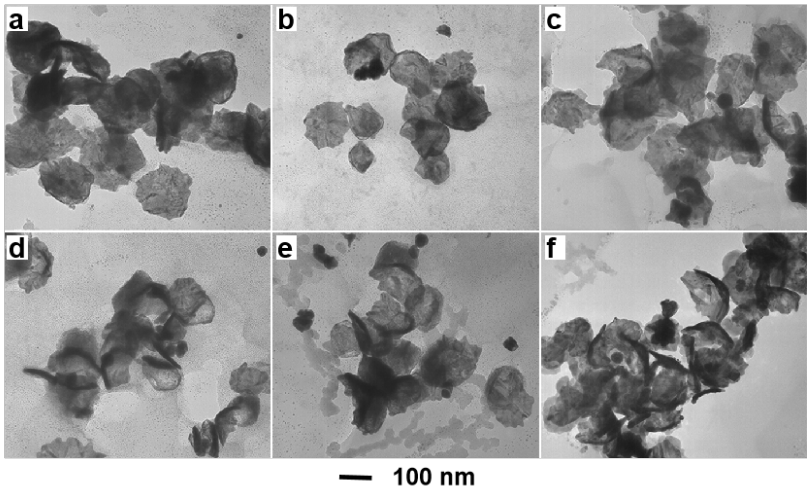

Figure S9. TEM images of nanoparticles obtained using the same synthetic protocol as (**a**–**c**) AuCu PHNSs and (**d**–**f**) AuAgCu PHNSs, but with varied etching treatments: (**a**,**d**) $HAuCl_4$, (**b**,**e**) $HAuCl_4$ + KCl, and (**c**,**f**) $HAuCl_4$ + acetic acid.

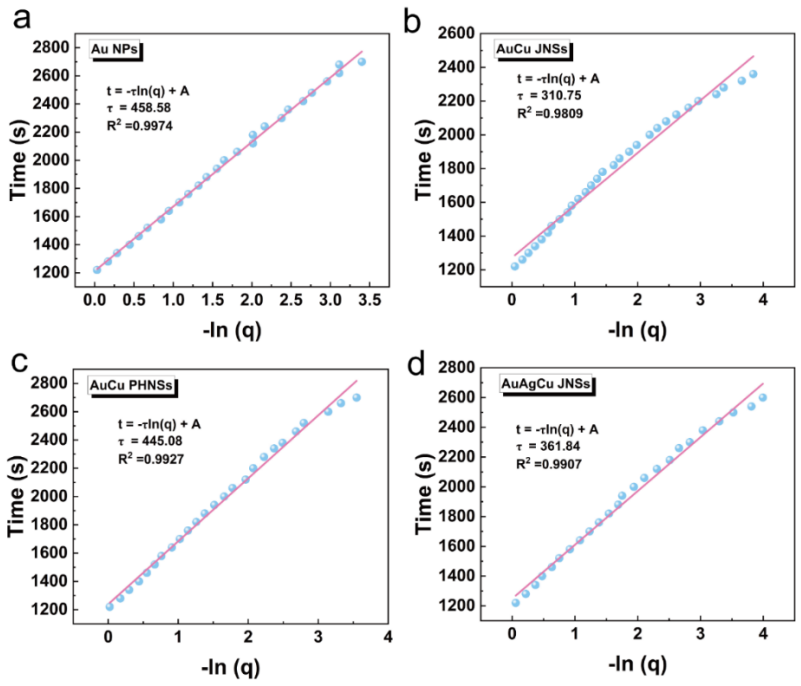

Figure S10. Determining the thermal transfer time constant (τ) of the system by plotting linear data from cooling times: (**a**) Au NPs; (**b**) AuCu JNSs; (**c**) AuCu PHNSs; (**d**) AuAgCu JNSs. Laser wavelength: 808 nm.

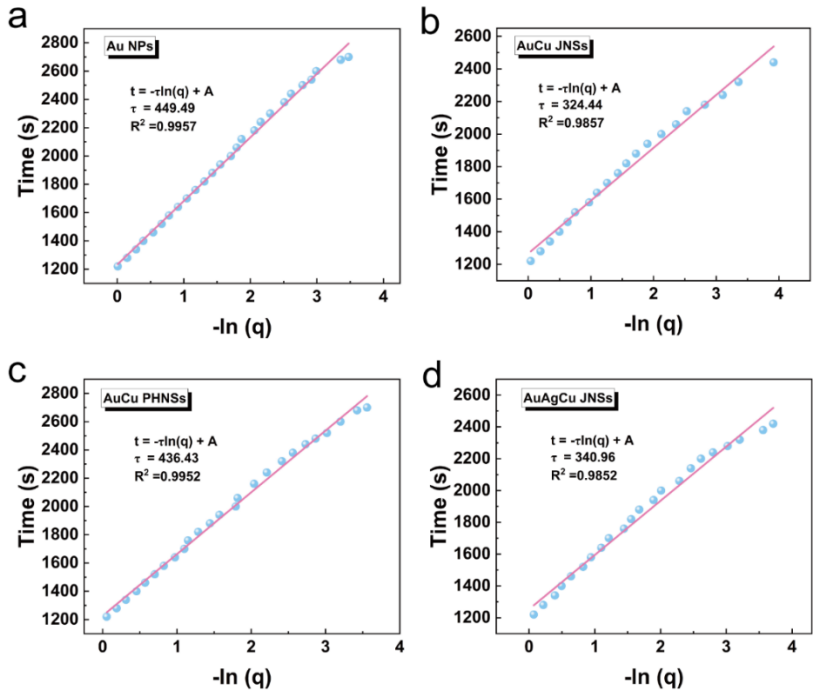

Figure S11. Determining the thermal transfer time constant (τ) of the system by plotting linear data from cooling times: (**a**) Au NPs; (**b**) AuCu JNSs; (**c**) AuCu PHNSs; (**d**) AuAgCu JNSs. Laser wavelength: 1064 nm.

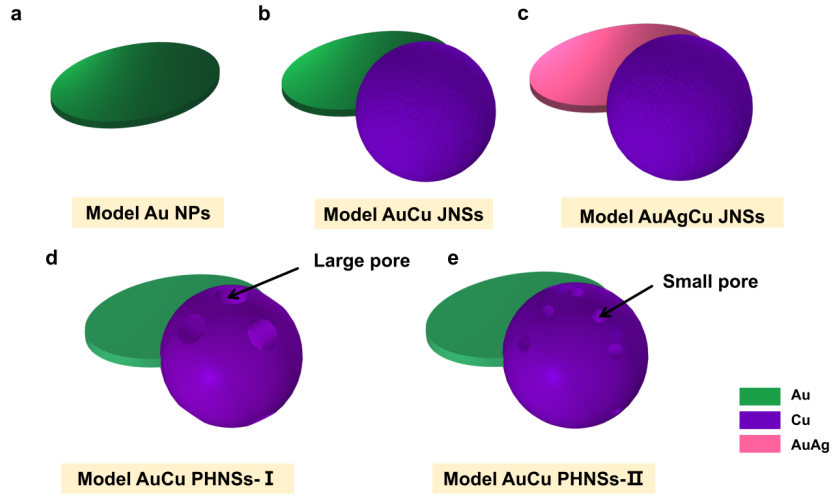

Figure S12. The model schematics of (**a**) Model Au NPs; (**b**) Model AuCu JNSs; (**c**) Model AuAgCu JNSs; (**d**) Model AuCu PHNSs-I and (**e**) Model AuCu PHNSs-II.

Table S1. XRD results of AuCu-based products in the current study.

Sample	Two Theta (Degree)									
	(111)		(200)		(220)		(311)		(222)	
	Au/Ag	Cu	Au/Ag	Cu	Au/Ag	Cu	Au/Ag	Cu	Au/Ag	Cu
AuAgCu PHNSs	38.1	43.1	44.5							
AuCu PHNSs	38.2	43.2	44.5	50.2	64.5	74.0	77.6	89.7	81.7	
AuAgCu JNSs	38.1	43.1	44.4	50.3	64.6	74.0	77.6	89.8	81.7	
AuCu JNSs	38.1	43.2	44.3	50.3	64.8	74.0	77.7	89.9	81.8	
Au (PDF #04-0784)	38.2	/	44.4	/	64.6	/	77.6	/	81.7	/
Ag (PDF #04-0783)	38.5	/	44.3	/	64.4	/	77.5	/	81.5	/
Cu (PDF #04-0836)	/	43.3	/	50.4	/	74.1	/	89.9	/	95.1

Table S2. Summary of the relative peak areas (%) for each split B.E. peak and the parameters used to fit the Cu 2p, Cu LMM, and Au 4f high-resolution XPS spectra.

Sample	Element	Oxidation State	Spectral Line	B.E. (eV)	FWHM (eV)
AuCu PHNSs	Cu	I	$2p_{3/2}$	932.31	1.40
			$2p_{1/2}$	952.18	2.27
		II	$2p_{3/2}$	934.17	2.61
			$2p_{1/2}$	954.34	2.86
		/	Cu-LMM *	915.12	6.22
	Au	0	$4f_{7/2}$	84.77	3.21
			$4f_{5/2}$	88.71	3.09
AuAgCu PHNSs	Cu	I	$2p_{3/2}$	932.08	1.03
			$2p_{1/2}$	951.96	2.17
		II	$2p_{3/2}$	933.99	4.70
			$2p_{1/2}$	954.63	3.54
		/	Cu-LMM *	916.07	8.33
	Au	0	$4f_{7/2}$	84.01	0.77
			$4f_{5/2}$	87.68	0.76
AuAgCu JNSs	Cu	I	$2p_{3/2}$	932.20	1.21
			$2p_{1/2}$	952.05	1.48
		II	$2p_{3/2}$	933.45	3.70
			$2p_{1/2}$	953.19	4.76
		/	Cu-LMM *	916.18	8.03
	Au	0	$4f_{7/2}$	83.80	0.80
			$4f_{5/2}$	87.48	0.83
	Ag	0	$3d_{5/2}$	367.94	0.86
			$3d_{3/2}$	373.94	0.82
AuCu JNSs	Cu	I	$2p_{3/2}$	932.30	1.34
			$2p_{1/2}$	952.12	1.67
		II	$2p_{3/2}$	933.81	3.05
			$2p_{1/2}$	953.34	5.47
		/	Cu-LMM *	914.82	5.96
	Au	0	$4f_{7/2}$	83.93	0.78
			$4f_{5/2}$	87.61	0.83

* Kinetic Energy.

Table S3. Photothermal conversion efficiency of Au NPs, Au-Cu JNSs, Au-macro Cu JNSs, Au-Ag-Cu JNSs, and Au-Ag-meso Cu JNSs.

Material	Photothermal Conversion Efficiency	
	Laser: 808 nm	Laser: 1064 nm
Au NPs	69.49%	32.11%
AuCu JNSs	77.86%	30.40%
AuCu PHNSs	65.19%f	31.72%
AuAgCu JNSs	69.17%	31.64%
AuAgCu PHNSs	67.15%	31.35%

Table S4. Comparative photothermal conversion performance of Au-based photothermal materials.

Material	Laser Wavelength (nm)	Power Density (W cm^{-2})	Photothermal Conversion Efficiency (%)	Reference
AuAg NCs	808	1	31.2	[1]
Au-Ag@Au NCs	808	1	36.5	[1]
Au@Pt	808	1	55.8	[2]
ATP@Au-CuNPs	808	2	59.3	[3]
Vap@Ag/AuNSs	808	1.5	41.6	[4]
Au-Ag-GO_x HTNs	1064	1.5	32.38	[5]
CuS-Au	1064	1	36.5	[6]
TA-Si-Au	1064	1	24.1	[7]
Au NR@ZIF-8	1064	1	39.2	[8]
Pt-covered Au@ZIF-8	1064	1	40.2	[8]
AuAgCu PHNSs	808	1	67.15	*
AuAgCu PHNSs	1064	1	31.35	*

* This work.

References

1. Jiang, T.; Song, J.; Zhang, W.; Wang, H.; Li, X.; Xia, R.; Zhu, L.; Xu, X. Au–Ag@Au Hollow Nanostructure with Enhanced Chemical Stability and Improved Photothermal Transduction Efficiency for Cancer Treatment. *ACS Appl. Mater. Interfaces* **2015**, *7*, 21985–21994. https://doi.org/10.1021/acsami.5b08305.
2. Bu, Y.; Huang, R.; Li, Z.; Zhang, P.; Zhang, L.; Yang, Y.; Liu, Z.; Guo, K.; Gao, F. Anisotropic Truncated Octahedral Au with Pt Deposition on Arris for Localized Surface Plasmon Resonance-Enhanced Photothermal and Photodynamic Therapy of Osteosarcoma. *ACS Appl. Mater. Interfaces* **2021**, *13*, 35328–35341. https://doi.org/10.1021/acsami.1c07181.
3. Song, Q.; Liu, Y.; Zhang, P.; Feng, W.; Shi, S.; Zhou, N.; Chu, X.; Shen, J. Au–Cu Bimetallic Nanostructures for Photothermal Antibacterial and Wound Healing Promotion. *ACS Appl. Nano Mater.* **2022**, *5*, 8621–8630. https://doi.org/10.1021/acsanm.2c02152.
4. Zhu, R.; Li, Y.; Zhang, X.; Bian, K.; Yang, M.; Cong, C.; Cheng, X.; Zhao, S.; Li, X.; Gao, D. Vapreotide-Mediated Hierarchical Mineralized Ag/Au Nanoshells for Photothermal Anti-Tumor Therapy. *Nanotechnology* **2019**, *30*, 055602. https://doi.org/10.1088/1361-6528/aaf0db.
5. Xu, M.; Lu, Q.; Song, Y.; Yang, L.; Ren, C.; Li, W.; Liu, P.; Wang, Y.; Zhu, Y.; Li, N. NIR-II Driven Plasmon-Enhanced Cascade Reaction for Tumor Microenvironment-Regulated Catalytic Therapy Based on Bio-Breakable Au–Ag nanozyme. *Nano Res.* **2020**, *13*, 2118–2129. https://doi.org/10.1007/s12274-020-2818-5.
6. Wang, Z.; Yu, N.; Li, X.; Yu, W.; Han, S.; Ren, X.; Yin, S.; Li, M.; Chen, Z. Galvanic Exchange-Induced Growth of Au Nanocrystals on CuS Nanoplates for Imaging Guided Photothermal Ablation of Tumors. *Chem. Eng. J.* **2020**, *381*, 122613. https://doi.org/10.1016/j.cej.2019.122613.
7. Sun, L.; Chen, Y.; Gong, F.; Dang, Q.; Xiang, G.; Cheng, L.; Liao, F.; Shao, M. Silicon Nanowires Decorated with Gold Nanoparticles via *in situ* Reduction for Photoacoustic Imaging-Guided Photothermal Cancer Therapy. *J. Mater. Chem. B* **2019**, *7*, 4393–4401. https://doi.org/10.1039/C9TB00147F.
8. Chen, M.M.; Hao, H.L.; Zhao, W.; Zhao, X.; Chen, H.Y.; Xu, J.J. A Plasmon-Enhanced Theranostic Nanoplatform for Synergistic Chemo-Phototherapy of Hypoxic Tumors in the NIR-II Window. *Chem. Sci.* **2021**, *12*, 10848–10854. https://doi.org/10.1039/d1sc01760h.